Charge-state dependence of image-charge acceleration of convoy electrons in fast, grazing collisions of carbon ions with a silicon (100) surface

H. Lebius,* R. Minniti, J. Y. Lim, and S. B. Elston
University of Tennessee, Knoxville, Tennessee 37996-1200
and Oak Ridge National Laboratory, Oak Ridge, Tennessee 37831-6377
(Received 10 May 1996)

Electron emission distributions, triply differential in emission energy and angles, are presented for collisions of singly through quadruply charged C ions impinging on a Si(100) surface, with ion energies between 3.6 and 6.0 MeV and grazing angles of incidence between 0.1° and 1.0°, respectively. The electron emission spectra measured under these conditions confirm previous reports of a shift of the convoy electron peak toward higher energy due to surface wake or image acceleration. Detailed angular distributions demonstrate a shift of convoy emission towards larger angles with respect to the surface plane, which is further evidence of the acceleration of emitted electrons by the surface wake potential. In addition, we observe the peak energy shift to depend upon the incident ion charge state for the higher projectile velocity (~4.5 a.u.). This dependence may be understood as a consequence of incomplete projectile charge equilibration at the time of convoy electron production. The charge-state dependence is not observed at the lower collision velocity (~3.5 a.u.). [S1050-2947(96)09811-3]

PACS number(s): 34.50.Dy, 79.20.Rf

I. INTRODUCTION

Ion scattering phenomena at surfaces provide the basis for a number of surface-analytic methods [1]. Interpretation of the results of such techniques relies on an accurate understanding of the ion-surface interaction, examinations of which are under way both experimentally [2–11] and theoretically [12–16]. The present work belongs to a class of experiments that utilize fast ions directed nearly parallel to the surface, so the velocity component perpendicular to the surface is sufficiently small that the ion can reflect from the surface [8–11]. During such a collision, the projectile interacts with a large number of target electrons and ion cores, allowing processes like electron capture to the continuum (ECC), electron loss to the continuum (ELC), and binary encounter ionization (BEI). The first two processes contribute to the so-called convoy electron peak [17], a group of electrons traveling with (nearly) the same vector velocity as the ion. The low emission velocity of convoy electrons relative to the projectile ion results in a laboratory-frame angular distribution, which is strongly peaked in the forward direction and which in turn makes efficient collection of convoy electrons possible. In contrast to the related ion-atom collision processes (ECC and ELC), convoy electrons produced in ion-surface collisions are not emitted solely in the Coulomb field of the ion; they additionally experience a repulsion from the dynamic surface wake potential induced by the passing ion [18]. The resultant acceleration has been found to be the source of a shift in the energy position of the convoy peak [8,18]. Indeed, a low emission velocity relative to the projectile translates into a low velocity relative to the projectile-induced surface wake, making the energy and angular distribution of convoy electrons a sensitive probe of that dynamic image potential, or wake. This paper will present observations of convoy electron emission that employ heavy ions, permitting a range of projectile charge states, and that provide evidence of a dependence of the convoy electron acceleration shift upon the incoming projectile charge in relatively fast collisions. This effect will be interpreted as a consequence of incomplete charge-state equilibration when the convoy electron emission process occurs.

II. APPARATUS AND METHOD

Two orthogonal views of the heart of the apparatus are shown in Fig. 1. A collimated ion beam is directed onto a single-crystal target surface at a grazing angle. Electrons produced in the ion-surface interaction and emitted in the forward direction with respect to the incoming ion trajectory are energy analyzed by an emission angle-resolving electrostatic spectrometer. Because the electrons are emitted near the entrance focal point of the spectrometer, the angular distribution of those passing the exit aperture closely matches the emitted distribution [19]. The energy-analyzed electrons are detected with a two-dimensional position sensitive detector [20], where the position information yields two orthogonal angles of the emission direction. We are thereby able to measure the triply differential (in energy and both ejection angles) electron emission distribution. Ions missing the target or scattered through angles less than nine degrees are transmitted through a hole in the outer sector of the spectrometer and are collected in a well-shielded and suppressed Faraday cup.

The experiment is housed in a bakable UHV chamber pumped by two turbomolecular pumps in series and by a supplemental cryopump. This arrangement produces residual

*Present address: University of Stockholm, Stockholm, Sweden.

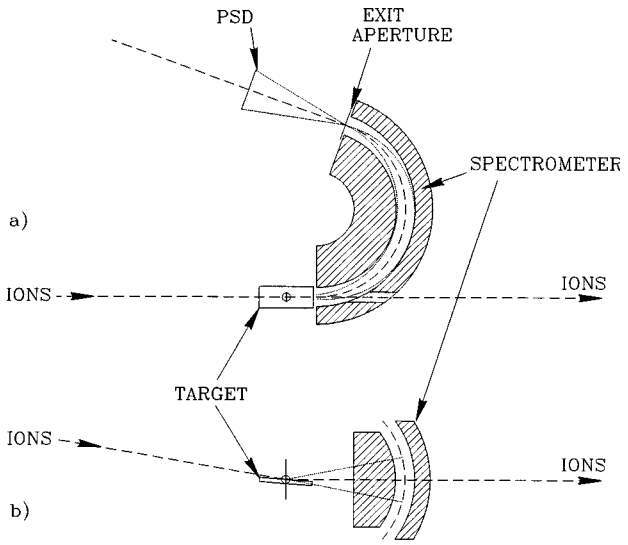

FIG. 1. Side (a) and bottom (b) view of arrangement of crystal target and electron spectrometer, approximately to scale. The spectrometer cross section is taken in the plane of the central ray in (a) and in a plane containing the sector center-of-curvature and parallel to the specular scattering plane in (b).

gas pressures as low as 1×10^{-10} Torr. A differential turbomolecular pumping stage between the main chamber and the beamline (with a pressure near 10^{-8} Torr) maintains the chamber pressure below 3×10^{-10} Torr with 3-mm pumping holes concentric with the beam axis.

The ion beam was supplied by the EN Tandem Van de Graaff Accelerator Facility of the Physics Division at Oak Ridge National Laboratory. For the experiments described here we used carbon ions with charge states one through four and kinetic energies of 3.6 and 6.0 MeV, which were collimated by an upstream aperture of 1 mm diam. and a downstream slit with a width of 0.2 mm and a height of 1 mm, separated by 150 cm to provide an angular divergence in the horizontal plane of less than 0.4 mrad (half angle) and a beam diameter at the location of the target of less than 0.4 mm.

The silicon target crystal is affixed by tantalum clips to two tantalum supports. The crystal supports are mounted on an insulating (Al_2O_3) base and serve as electrical contacts along the two edges of the crystal which are parallel to the incident-beam direction, permitting connection of a low-voltage DC power source for direct Ohmic heating of the target, or of a picoammeter for measuring currents intercepted by the target when an ion beam is incident. All contact of target material with stainless steel is avoided to minimize contamination of the crystal surface with nickel from stainless steel parts and tools. The target base is mounted on a goniometer head, which is in turn mounted on a manipulator with five degrees of freedom, allowing alignment of the ion beam, the center of the surface, and the entrance focus of the spectrometer at one point. In addition, the target mounting permits adjustment of the ion-beam angle of incidence and of perpendicularity between the incident beam and the axis of the incidence-angle rotation. Because the incidence-angle adjustment is achieved by a linear motion feedthrough, the angle is calibrated by measuring the deflection of a laser beam reflected from the surface of the crystal for different positions of the incidence-angle motion feedthrough. The grazing angle of incidence is defined here as the complement of the usual angle of incidence and is measured between the incident beam and the surface in the plane containing the incident beam and the surface normal. As the crystal intersects a minimum beam cross section when its surface is parallel to the beam axis, it is relatively easy to determine the zero of the grazing incidence angle by measuring the current on the surface produced by the incoming ion beam as a function of the position of the incidence-angle feedthrough; if the crystal is tilted away from the zero direction, it intersects more of the ion beam (the crystal current rises) and the current in the Faraday cup decreases, leading to a minimum in the surface current and a maximum in the current measured in the Faraday cup. In the measurements presented here, it was possible to reliably reproduce this angle to within 0.05°.

The parent single-crystal wafers of the silicon targets used in the present measurements were specifically cut and certified by x-ray diffraction measurements performed by the manufacturer and donor [21] to provide an average crystal surface inclined at 0.4° to the (100) plane; approximately regular terrace steps would then be spaced by ~20 nm on average. Using additional orientation information supplied with the parent wafers, it was possible to mount the final target crystals so that the ion beams passed parallel to the average terrace edges. Assuming an orientation precision better than 5°, the distance between adjacent terrace edges encountered by the ions exceeded 200 nm on the average.

In order to remove the initial silicon-oxide layers and to anneal the surfaces, the targets were heated by passing a current through the bulk crystal, and by following a prescription developed by Swartzentruber *et al.* [22] Surface temperatures were measured with an optical pyrometer. The process typically consisted of an outgassing cycle at 400–500 °C for a few hours and then by a high-temperature ''flash'' for 10–30 s near 1000 °C, followed by about 10 min of slow, controlled cooling to the ambient temperature of surrounding hardware. After such treatment, the crystal was found to be useable for at least 20 h before requiring further heating, during which interval the coverage of the surface with residual gas atoms was small, as judged by changes in observed electron emission spectra and in a sense defined more precisely in the Results and Discussion section.

A 160° spherical electrostatic analyzer, described in detail elsewhere [19], is used to analyze electrons emitted in the forward direction during the ion-surface interaction. The analyzer mounting permits rotation about two perpendicular axes intersecting at the entrance focal point. With a drift region of 61 mm between the 1 mm diameter exit aperture and the microchannel plate entrance, the resistive anode-encoded position-sensitive detector (PSD) views an angular cone with a half angle of about 12° and angular resolution of about 0.5°. However, the angular acceptance of the analyzer itself is restricted by interception of electron trajectories at the spherical sectors and field terminators, leading to overall acceptance half angles of about 6° in the deflection plane and 12° in the orthogonal direction [19]. The energy resolution, $\Delta E/E$, provided by this arrangement is about 1% full width at half maximum (FWHM). The digital output of the position-computing electronics as well as digital-to-analog converter control of the analyzer deflection voltage supply

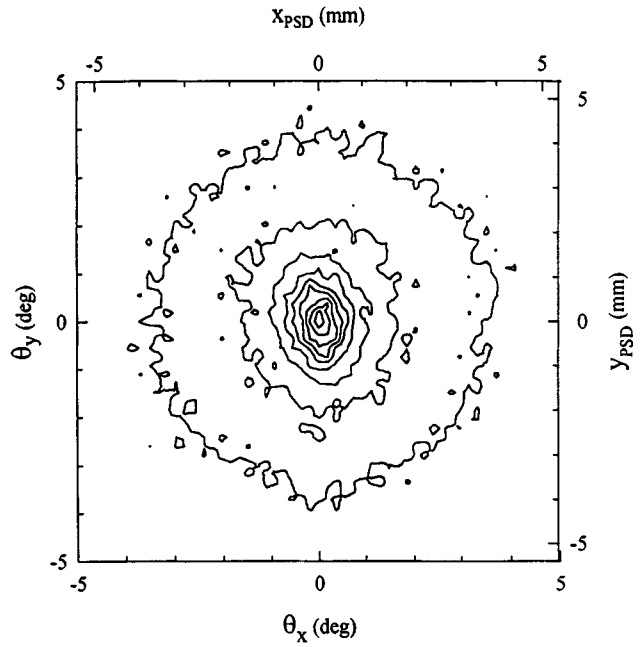

FIG. 2. Angular distribution of convoy electrons produced by C^+ ions with a kinetic energy of 3.6 MeV passing through a 20-μg/cm^2-thick carbon foil. The spectrometer pass-energy was 157.2 eV; see text. Contours of equal emission intensity are equally spaced between zero and maximum count rate.

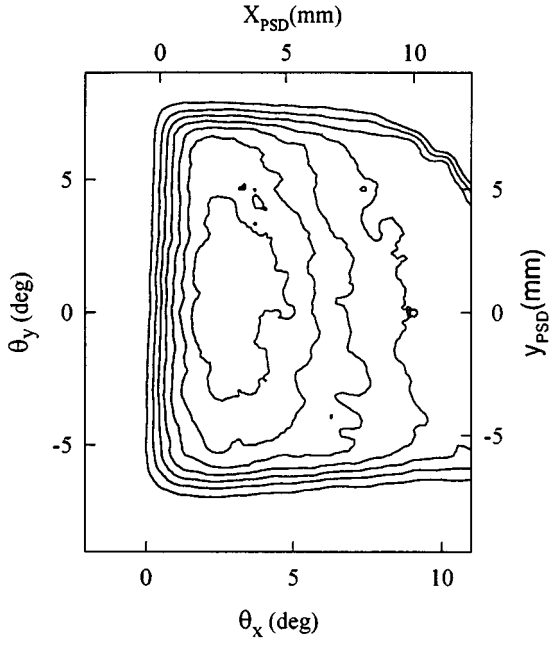

FIG. 3. Angular distribution of convoy electrons produced by C^+ ions with a kinetic energy of 3.6 MeV incident upon a silicon(100) surface with a grazing angle of 0.15°. The spectrometer pass-energy was 246 eV. Contours of equal emission intensity are equally spaced between zero and maximum count rate.

were interfaced to an IBM-compatible personal computer for data acquisition.

Periodic tests of the performance and energy calibration of the electrostatic electron analyzer were performed by withdrawing the surface mounting and observing the convoy electron emission produced by ions transmitted through a self-supporting 20-μg/cm^2 carbon foil positioned normal to the incident ion beam at the analyzer entrance focus. Figure 2 displays contours of equal convoy electron emission intensity produced by 3.6 MeV C^+ ions and observed with the analyzer positioned at 0° with respect to the incident ion direction and tuned to a pass energy of 157 eV. The emission contours are plotted in the rectangular position coordinates, x and y, natural to the PSD; for convenience, those coordinates are also converted in the figure to the two rectangular components of the polar emission angle, θ_x and θ_y. The clearly circular contours demonstrate azimuthal isotropy, as expected for a collision geometry which is azimuthally symmetric about the incident beam, and faithful representation of the same by the apparatus. The convoy electron peak energy isotachic to C ions with a kinetic energy of 3.6 MeV is 164.6 eV. The observed peak energy is 157.2 eV (as in Fig. 2) as a consequence of two phenomena: (i) the mean attenuation length of ~160 eV electrons in a carbon foil [23] is much less than the thickness of the foil target used. As a result, the observed emission is of convoy electrons produced in a ~1-nm-thick ''last layer.'' (ii) Electronic stopping power-related kinetic-energy loss produces a deceleration of the ions responsible for convoy electron production in this last layer of the foil by ~155 keV [24]. The observed peak energy is thus, within the analyzer resolution and precision of the accelerator energy (typically 1 part in 10^3), in agreement with the expected value of 157.4 eV. Foil target convoy peak energy measurements, corrected for target energy loss, were used throughout this work as a double-check of the ion kinetic energy.

III. RESULTS AND DISCUSSION

A typical result for the convoy peak angular distribution, analogous to Fig. 2 but with a silicon surface replacing the foil target, is shown in Fig. 3. For this measurement, 3.6-MeV C^+ ions were incident upon a Si(100) surface at a grazing angle of 0.15°. The electron analyzer pass energy was 246 eV, slightly higher than the observed convoy peak energy for this case. As in Fig. 2, the two detector coordinates x and y have been translated into rectangular components of the polar emission angle, measured in the surface scattering case with respect to the asymptotic trajectory of a perfectly specularly reflected outgoing ion. θ_x denotes the component in the plane defined by the surface normal and the incoming ion trajectory (i.e., the scattering plane), and will subsequently be referred to as the *in-plane component* of the polar emission angle. θ_y is the component parallel to the surface plane, or normal to the scattering plane, and will be referred to as the *out-of-plane component*.

The angular distribution is clearly broader in both angles θ_x and θ_y than in the previous case of ion-foil interactions. The distribution in the out-of-plane component is sufficiently broad that it is limited by the angular acceptance of the spectrometer; consequently, Fig. 3 provides only a lower limit for the width of the distribution in θ_y, and the extent of the emission in this direction was not explored in the measurements presented here. The distribution in the in-plane component, θ_x, is asymmetric, with a long tail towards higher angles away from the surface, and is shown in further detail in Fig. 4, for 3.6-MeV C^+ ions incident upon a Si(100) sur-

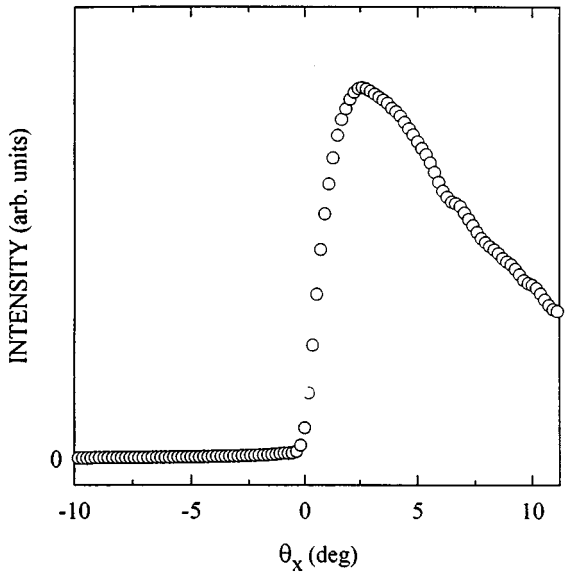

FIG. 4. Polar angle (in-plane component) distribution of convoy electrons emitted in interactions of 3.6-MeV C^+ with a Si(100) surface at a grazing angle of 0.15°, derived from the data of Fig. 3 (see text).

face at a grazing angle of 0.15°. At small angles θ_x corresponding to electron emission nearer the surface than the specular reflection direction, there is a sharp cut-off, since for such emission angles the electrons either pass slightly above the surface and become attenuated by multiple collisions in the valence electron ''selvage,'' or enter the crystal and become lost to multiple collisions within the bulk. On the positive side of the θ_x distribution, the peak is substantially broader. While it is to be expected that repulsion of convoy electrons by the surface wake potential should result in a deflection of the angular distribution peak, the combined effects of the near-surface cutoff produced by multiple scattering in the selvage and of the spectrometer transmission function upon the angular emission peak are not understood at a level adequate to extract quantitative information about the wake potential from the angular distribution at the present level of development of the measurement.

To obtain emission spectra, as shown in Fig. 5 for 6-MeV C^{2+} ions incident at an angle of 0.22° to a Si(100) surface, detector events are integrated over that portion of the out-of-plane polar angle (θ_y) range which is unrestricted by the spectrometer acceptance and accumulated as a function of the in-plane component of polar angle, θ_x, and spectrometer pass-energy, E. Figure 5(a) displays contours of equal electron intensity seen by the PSD as a function of E and θ_x. The events in Fig. 5(a) are integrated over the FWHM of the in-plane (θ_x) angular distribution observed at the convoy peak energy [near 330 eV in Fig. 5(a)] to produce Fig. 5(b) of the emitted electron intensity, integrated over the previously specified angular range, versus electron emission energy. Figure 5 shows two distinct electron populations: convoy electrons at ~330 eV, produced in electron capture and loss to continuum processes, and binary encounter electrons in the range 500 to 800 eV, produced in direct collisions of the projectile with target valence electrons. While the convoy peak observed in ion-gas and ion-bulk-solid collisions is velocity matched, or isotachic, with the projectile

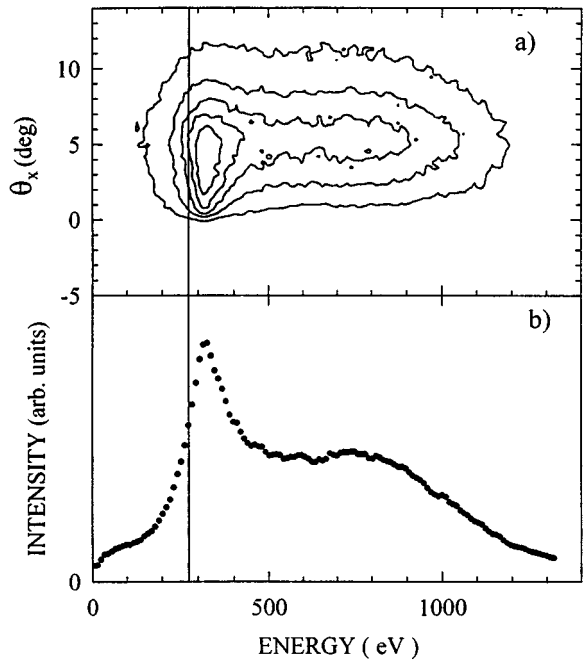

FIG. 5. Emission distribution of electrons emitted in collisions of 6.0-MeV C^{3+} ions directed toward a Si(100) surface with a grazing angle of 0.22°. The emission is shown in (a) as contours of isointensity, equally spaced between zero and the convoy peak rate and doubly differential in the in-plane component of polar angle (θ_x, see text) and emission energy, and in (b) as a spectrum of electrons emitted within (i.e., integrated over) an angular range as specified in the text. The isotachic emission energy is shown by a vertical ruling in both figures.

beam, a strong postcollision interaction between the convoy electrons and the surface wake potential induced by the passing charged projectile repels the emitted electron and results in a higher emission energy [8,18] and a larger mean emission angle θ_x. This accounts for a peak location at ~330 eV, compared with the isotachic value (marked by the vertical line in Fig. 5) of 274 eV for 6-MeV C ions. Thus we infer that the wake potential accelerates or shifts the convoy electrons by 64 eV. In addition, the convoy electrons are accelerated away, or deflected in direction, from the surface, as can be clearly seen in Fig. 5(a) where the maximum of the convoy peak distribution in θ_x is a few degrees further from the surface plane than the direction of a specularly reflected ion.

Detailed spectra of the convoy peak region for a variety of incoming carbon projectile charge states, incident at a common surface grazing angle of 0.22°, and for kinetic energies of 3.6 and 6 MeV (corresponding to projectile velocities of 3.5 and 4.5 a.u., respectively) are shown in Fig. 6. The data of this figure were integrated over an emission angle range as in Fig. 5 for the out-of-plane component (θ_y), over an in-plane component (θ_x) from 0° to 3.6°, and have been peak normalized to facilitate comparison of the peak locations. These data have also been divided by emission energy to correct for the energy-dependent spectrometer transmission and thus (apart from peak normalization) reflect peak shapes and positions of the singly differential emission probability rather than emission intensity, as seen by the detector. From the centroid values E_c of Gaussian functions fit by least-

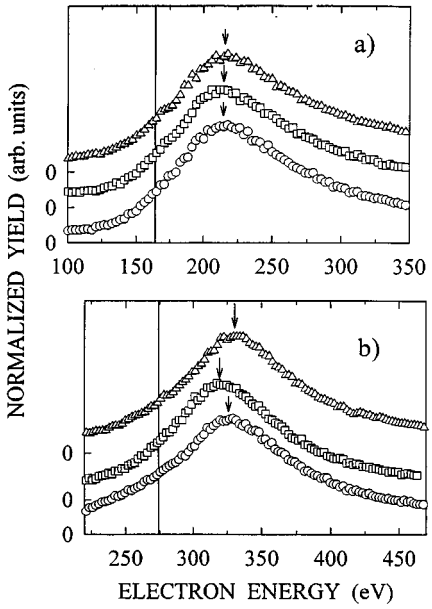

FIG. 6. Detailed emission spectra, corrected for spectrometer transmission efficiency, of the convoy peak region for (a) 3.6-MeV and (b) 6.0-MeV carbon ions having initial charge states 1+ (circles), 2+ (squares), and 3+ (triangles) incident with a grazing angle of 0.22° upon the same silicon(100) surface. Charge state 4+ is omitted for clarity. The vertical rulings indicate the isotachic emission energy.

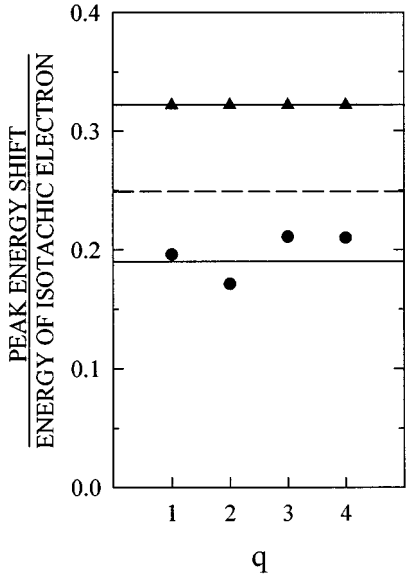

FIG. 7. Dependence of the fractional shift of convoy peak energy, as defined in the text, upon incident charge state, q, and energy, for a grazing incidence angle of 0.22° with silicon(100) and kinetic energy 3.6 MeV (triangles) and 6.0 MeV (circles). $1/v_p^2$ scaling of the peak shift, normalized to the 3.6 MeV data, would produce results clustered about the solid horizontal lines, whereas $1/v_p$ scaling would predict 6.0-MeV data clustered about the dashed horizontal line.

squares minimization to the peaks of these spectra, shifts $\Delta E = E_c - E_i$ of the convoy peak from the expected, isotachic energy E_i were obtained. The peak shifts, expressed as fractions of the isotachic energy, and their dependence on incident projectile charge state and energy, are summarized in Fig. 7. For a projectile energy of 3.6 MeV, the convoy peak was invariably observed at 216 eV, amounting to a shift of 52 eV independent of the incident charge state to within the accuracy of the spectrometer energy calibration. However, in the case of 6-MeV projectiles, the shift was observed to be reproducibly and significantly dependent on the initial projectile charge state: the convoy peak energy varies between 321 eV for C^{2+} ions and 332 eV for C^{4+} ions, corresponding to shifts between 47 and 58 eV, respectively. Deriving the singly differential spectra from the triply differential raw data sets using reasonably different integrations (for example, for θ_x integrated over the FWHM of the convoy peak vs over the unobstructed angular field of view of the spectrometer) does not appreciably affect the peak positions and shifts; in fact, the plotting symbols displayed in Fig. 7 overlap the range of values obtained by several such choices of angular integrations. These results have been reproduced in separate beamtimes with different Si(100) surface samples, and with the order of the incident charge states reversed in the two experiments to minimize possible effects of time-dependent surface coverage and/or radiation damage. Further specification of the possible effect of accumulation of surface contamination over the course of the measurements was obtained by observing the electron emission spectrum produced by incident 3.6-MeV C^{2+} immediately prior and subsequent to a surface flash treatment which followed a previous treatment by approximately 13 h. No change in convoy peak position, width, or shape was observed. The primary change noted following this heat treatment was a ~5% decrease in the emission intensity ratio of the convoy peak at 216 eV to binary encounter emission at 500 eV.

The convoy electron acceleration, or peak shift, is governed by the amplitude of the surface wake potential and by the evolution thereof as that wake responds to changes in both position and charge state of the projectile. The projectile charge fluctuates during the course of the collision and, in the grazing collisions studied here, is mainly determined by competition between projectile-ionizing collisions and capture from target core states. It may be expected that with the large number of ion-target interactions that occur in grazing ion-surface collisions, a charge equilibration process will occur leading to a final projectile charge state that is independent of the initial, incident charge state, in a manner such as occurs in ion collisions with thick, bulk solid targets. The shifts of the convoy peak produced by the slower (3.6 MeV) ions shown in Fig. 7 are, within the uncertainties of the measurement, independent of incident projectile charge state, implying that the mean projectile charge at the moment of convoy production, averaged over an ensemble of incident ions having a given initial charge state, is nearly independent of the actual initial value. The presence of a dependence for the faster (6 MeV) ions suggests that such equilibration is not fully achieved for all incident charge states at the point of maximum convoy production probability, if at all, or, in other words, the mean projectile charge at the production point is not independent of the incident charge state. In this sense, it is not surprising that a charge state dependence is observed, but the nonmonotonic nature of that dependence remains to be understood. In the absence of more detailed information, as would be available from emission measure-

ments performed in coincidence with the exiting ion charge state and scattering angle, for example, it is only possible to specify that such nonmonotonicity is likely to develop on the way into the collision, prior to the establishment of charge state equilibrium. It also remains to rule out the possibility that a metastable component of the incoming beam may contribute to an anomalous result for incident 6-MeV C^{2+} ions. The latter seems unlikely in view of the complete lack of such an anomaly for 3.6-MeV projectiles, with a collision velocity only ~25% lower, and in addition because it might be expected that metastables would strip to higher charge states more quickly, thereby producing larger convoy accelerations rather than smaller peak shifts as observed.

Any mechanism proposed to explain the observed incident charge state dependence is likely to be quite sensitive to the specific trajectory followed by a projectile of a given initial charge state, and to the electronic environment sampled by that trajectory. Consequently, a direct quantitative comparison between the present results and those of Kimura, Tsuji, and Mannami [8], who also employed carbon ions in the energy range studied here, is not entirely appropriate as their SnTe (100) target should produce different ion trajectories and surface wakes than those produced by the present Si(100) target. In addition, Kimura, Tsuji, and Mannami report a result for only a single charge state at the collision velocity (4.5 a.u.) at which we observe the effect of charge state on peak shift. However the shifts observed by Kimura, Tsuji, and Mannami for C^{3+} ions at 3.6 MeV and C^{4+} ions at 6 MeV scale with projectile velocity v_p in a similar way. The present charge-state-dependent data points for 3.6-MeV ions lie on a straight horizontal line, as seen in Fig. 7, corresponding to a fractional peak shift $\Delta E/E_i = 0.32$. Scaling this value by $1/v_p$ from the 3.6 MeV projectile case to 6 MeV leads to a fractional shift of 0.25, as shown by the dashed horizontal line in Fig. 7, whereas $1/v_p^2$ scaling produces a value of 0.19, shown by the lower solid line in Fig. 7. On average, considering all incident charge states, the data seem to favor a $1/v_p^2$ scaling of $\Delta E/E_i$. On the other hand, $\Delta E/E_i$ associated with charge states $q=3+$ and $4+$ exhibits velocity dependence intermediate between $1/v_p$ and $1/v_p^2$. The latter incident charge state is of relevance because it is most likely to remain near the expected mean equilibrium charge, which for bulk silicon is 3.8 and 4.3 at collison velocities corresponding to 3.6- and 6.0-MeV projectiles, respectively [25]. A $1/v_p^2$ dependence is consistent with the result of Kimura, Tsuji, and Mannami, who measured shifts of about 0.50 and 0.31 for 3.6-MeV C^{3+} and 6-MeV C^{4+} ions, respectively. The somewhat larger overall acceleration observed by them ($\Delta E/E_i \sim 0.31$, compared with our $\Delta E/E_i \sim 0.21$ for 6-MeV C^{4+}) is consistent with the higher Z of the constituent atoms of their SnTe surface, but may also reflect contributions from trajectory effects. Note that to extract a v_p dependence from the results of Kimura, Tsuji, and Mannami it is necessary to use data from different charge states ($q=3+$ at $v_p=3.5$ a.u. and $4+$ at 4.5 a.u.) but that the present results indicate that there is little difference between these particular charge states.

The incident charge-state (q) dependence we observe makes discussion of the velocity dependence of the wake-induced acceleration shift a complex matter: in the collision velocity range studied here, a different velocity dependence is indicated for different incident charges. Nevertheless, the velocity dependence provides a natural point of comparison with current theory of wake (or image) effects found in the literature. For example, Arista [15] recently provided results for the stopping force exerted on an ion passing at fixed distance outside a conducting surface, which force is produced by the wake field associated with that ion's image. The acceleration of convoy electrons in grazing ion-surface collisions arises from the same field, so in principle comparison could be made between the stopping force model calculations of that reference and the present convoy electron acceleration results. While the connection between the accelerating field and the acceleration or momentum transfer Δp clearly involves integrating the accelerating force over collision time, the velocity dependence of several factors entering the integration cloud the comparison. Burgdörfer [26] has estimated the convoy peak position by considering a Galilean transformation from projectile to laboratory frames of the projectile image-induced momentum transfer to a threshold continuum electron, $\Delta p \cong \sqrt{(Q-1)/2R_0}$ (atomic units). In this estimate, Q is the effective charge of the projectile and R_0 is the effective projectile-surface distance during the convoy electron ''acceleration phase.'' The result, $E_c = \frac{1}{2}(v_p + \Delta p)^2$, leads to $\Delta E/E_i = (1/v_p)2\Delta p + (1/v_p^2)\Delta p^2$. Direct comparison is hindered by incomplete knowledge of the projectile velocity dependence of Δp (i.e., of Q and R_0 in this simple picture) but one can infer from this expression of $\Delta E/E_i$ and from the observed velocity dependence—intermediate between $\sim 1/v_p$ and $\sim 1/v_p^2$—that Δp is relatively constant over the collison velocity range studied here, i.e., v_p between 3.5 and 4.5 a.u. The economy of expression afforded by this relatively simple estimate provides a good framework for a discussion of the broader problem of assessing the velocity dependence of $\Delta E/E_i$ (or of the related Δp). In this case, because the effective projectile charge Q evolves during multiple scatterings over the course of the collision, the value appropriate to evaluation of $\Delta p = \sqrt{(Q-1)/2R_0}$ most likely depends on v_p in a complicated and possibly non-power-law manner. A similar remark may be made about R_0: since it is anticipated that the continuum convoy state is populated in close encounters with target ion cores, the acceleration phase likely begins near the distance of closest approach to the surface layer of atoms, and this quantity is sensitive to collision velocity, angle of incidence, and details of the ion-surface potential [18,27].

IV. CONCLUSION

We have observed convoy electron emission from grazing interactions of carbon ions with a silicon surface in a triply differential measurement that confirms previous reports of a surface wake-induced shift of the convoy peak energy and provides detailed emission angular distributions. We further observe the peak shift to depend on the incident projectile charge state in a manner suggesting that the effective projectile charge controlling convoy electron production and acceleration, averaged over a large number of collisions, can vary with the incident charge in a nonmonotonic fashion which is sensitive to details of the ion trajectory and the electronic environment in the surface (''selvage'') region. Both models

and measurements of ion-surface scattering in this velocity regime that are designed to probe surface wake phenomena accordingly need to accurately account for the charge-state evolution of the projectile ion. Further, the observable charge-state dependence obscures the velocity dependence as an intrinsic signature of convoy electron acceleration. Planned measurements incorporating coincident detection of ions exiting the interaction region will permit selection of specific ion exit trajectories and charge states and straightforward determination of convoy electron yields. Combining such measurements obtained with the present and additional collision velocities will permit a stringent test of mechanisms that may be proposed to explain the present results.

ACKNOWLEDGMENTS

We wish to thank Mr. Jim Reed and the Silicon Products Department of Texas Instruments, Inc. for the donation of the silicon wafers vital to this experiment. Valuable conversations with J. Burgdörfer, C. Reinhold, and K. Kimura are gratefully acknowledged. The ion beams and other facilities were furnished by the EN Tandem Van de Graaff Accelerator Facility at the Oak Ridge National Laboratory. This work was supported by the National Science Foundation, and by the U.S. Department of Energy, Office of Basic Energy Sciences, under Contract No. DE-AC05-840R21400 with Lockheed Martin Energy Systems, Inc.

[1] See L. C. Feldman and J. W. Mayer, *Fundamentals of Surface and Thin Film Analysis* (North-Holland, Amsterdam, 1986), Chaps. 2–4, and references therein.
[2] F. W. Meyer, S. H. Overbury, C. C. Havener, P. A. Zeijlmans van Emmichoven, and D. M. Zehner, Phys. Rev. Lett. **67**, 723 (1991).
[3] J. Limburg, J. Das, S. Schippers, R. Hoekstra, and R. Morgenstern, Phys. Rev. Lett. **73**, 768 (1994).
[4] H. J. Andrä, A. Simionovici, T. Lamy, A. Brenac, and A. Pesnelle, Europhys. Lett. **23**, 361 (1993).
[5] J. P. Briand, L. de Billy, P. Charles, S. Essabaa, P. Briand, R. Geller, J. P. Desclaux, S. Bliman, and C. Ristori, Phys. Rev. Lett. **65**, 159 (1990).
[6] R. Köhrbrück, K. Sommer, J. P. Biersack, J. Bleck-Neuhaus, S. Schippers, P. Roncin, D. Lecler, F. Fremont, and N. Stolterfoht, Phys. Rev. A **45**, 4653 (1992).
[7] H. Kurz, K. Töglhofer, H. P. Winter, and F. Aumayr, Phys. Rev. Lett. **69**, 1140 (1992).
[8] K. Kimura, M. Tsuji, and M. Mannami, Phys. Rev. A **46**, 2618 (1992).
[9] L. F. de Ferrariis and R. A. Baragoila, Phys. Rev. A **33**, 4449 (1986).
[10] H. Winter, Europhys. Lett. **18**, 207 (1992).
[11] A. Koyama, Nucl. Instrum. Methods Phys. Res. Sect. B **67**, 103 (1992).
[12] J. Burgdörfer and F. Meyer, Phys. Rev. A **47**, R20 (1993).
[13] U. Wille, Surf. Sci. **307-309**, 874 (1994).
[14] U. Thumm, J. Phys. B **25**, 421 (1992).
[15] N. R. Arista, Phys. Rev. A **49**, 1885 (1994).
[16] T. Iitaka, Y. H. Ohtsuki, A. Koyama, and H. Ishikawa, Phys. Rev. Lett. **65**, 3160 (1990).
[17] M. Breinig *et al.*, Phys. Rev. A **25**, 3015 (1982).
[18] C. O. Reinhold, J. Burgdörfer, K. Kimura, and M. Mannami, Phys. Rev. Lett. **73**, 2508 (1994).
[19] R. deSerio, Rev. Sci. Instrum. **60**, 381 (1989).
[20] Quantar Technology, model 239G.
[21] Texas Instruments Silicon Products Department, Sherman, TX.
[22] B. S. Swartzentruber, Y.-W. Mo, M. B. Webb, and M. G. Lagally, J. Vac. Sci. Technol. A **7**, 2901 (1989).
[23] M. P. Seah and W. A. Dench, Surf. Interf. Anal. **1**, 2 (1979).
[24] L. C. Northcliffe and R. F. Shilling, Nucl. Data Tables **A7**, 233 (1970).
[25] V. S. Nikolaev and I. S. Dmitriev, Phys. Lett. **28A**, 277 (1968).
[26] J. Burgdörfer, in *Review of Fundamental Processes and Applications of Atoms and Ions*, edited by C. D. Lin (World Scientific, Singapore, 1993), pp. 514–614.
[27] C. O. Reinhold and J. Burgdörfer (unpublished).